Research Article | Vol. 27, No. 20 / 30 September 2019 / Optics Express 28660

Optics EXPRESS

High contrast thermal deflectometry using long-wave infrared time modulated integrating cavity source

LOGAN R. GRAVES,[1] HENRY QUACH,[1] R. JOHN KOSHEL,[1] CHANG-JIN OH,[1] AND DAE WOOK KIM[1,2,*]

[1] James C. Wyant College of Optical Sciences, University of Arizona, 1630 E. University Blvd., Tucson, AZ 85721, USA

[2] Department of Astronomy and Steward Observatory, University of Arizona, 933 N. Cherry Ave., Tucson, AZ 85719, USA

[*] letter2dwk@hotmail.com

Abstract: We introduce a scalable temporally modulated long-wave infrared source design. The design makes use of an array of resistive blackbody heating elements which radiate into a custom aluminum integrating cavity. The output of the box is a rectangular slit, built to match the traditional tungsten ribbon profile for an infrared deflectometry source. Temporal modulation allows for signal isolation and improved resilience to background fluctuations in an infrared deflectometry source. Infrared deflectometry measurements using the new source design and a traditional tungsten ribbon, both with similar radiant flux, were compared for a ground glass surface, an aluminum blank, and an aluminum blank under thermal load (150 °C). Signal-to-noise ratio was ~4 times higher for the new design and demonstrated improved source temporal stability and geometry. Further, the new design successfully measured the previously untestable hot aluminum flat. The new design improves infrared deflectometry and allows for high contrast thermal deflectometry measurements of optics under thermal load.

© 2019 Optical Society of America under the terms of the OSA Open Access Publishing Agreement

1. Introduction

As manufacturing methods continue to improve, a wider range of materials are being shaped into custom freeform surfaces for new optical applications. These materials, which include metals, glass, ceramics, and plastics, are turned into high performance optics using grinding and polishing methods, computer numeric control (CNC) diamond turning, sub-aperture polishing methods, 3D printing, and more [1–5]. To assure proper fabrication, advanced metrology technologies must be used. This allows for monitoring and guiding of the fabrication process, and final verification of the optical surface shape.

Typically, interferometry and deflectometry are used for high accuracy and precision metrology of freeform optics [4–7]. Interferometry is a null metrology method, which requires using a null optic as a reference measurement to the unit under test (UUT). For freeform optics in particular, computer generated holograms (CGH) have become highly attractive for use as a null optic as they can generate a freeform null and additionally can provide advanced alignment features [8]. Unfortunately, a CGH can only null a designed specific optical configuration, and they typically can be expensive to fabricate. Deflectometry is a non-null test method, in a which a source presents a known pattern which specularly reflects from the UUT and is recorded by a camera. By knowing the geometry of all components to high precision, the local slopes of the UUT can be determined and integrated to generate a reconstructed surface map. Particularly for extremely large optics, such as telescope optics, fabrication is typically achieved using grinding and polishing [5,9–11]. The grinding phase of generating optics offers a unique period during which rapid removal of material is performed, allowing for faster convergence to

#369651 https://doi.org/10.1364/OE.27.028660
Journal © 2019 Received 12 Jun 2019; revised 10 Sep 2019; accepted 11 Sep 2019; published 23 Sep 2019

Optics EXPRESS

the final desired surface shape, with removal rates being up to thousands of times faster than during polishing. During this period, the optical root mean square (RMS) surface roughness can range from hundreds of microns down to 1 micrometer, and the surface shape can change significantly. The rough surface is not specularly reflective to visible wavelengths, making measurements challenging. Utilizing an infrared system is a desirable solution to grinding phase metrology as the rough surface will be specularly reflective at longer wavelengths. While infrared interferometers exist which could achieve this measurement [12], the rapidly changing surface shape during the grinding phase requires equally rapidly changing custom null optics. Instead, deflectometry has been used with an infrared source to measure such rough surfaces [7,13].

A key challenge in designing infrared deflectometry systems is in the choice of a thermal source. Ideally, a deflectometry source will provide a high signal-to-noise ratio (SNR) for the system, while having high spatial modulation accuracy and capabilities and excellent stability. One possible source design is to apply current to a thin tungsten ribbon, which induces joule heating and creates a rectangular, pseudo-blackbody emitting source. By scanning the ribbon in orthogonal directions, a line scanning source is created. This ribbon design formed the basis for the scanning long-wave optical test system, SLOTS (Scanning Long-wave Optical Test System), which has been used extensively in infrared deflectometry, and the tungsten ribbon source, with minor variations, is still the traditional source used for infrared deflectometry [7,14]. However, a tungsten ribbon has some significant limitations when applied to deflectometry.

In a deflectometry system, any uncertainty in the shape and position of all components directly reduces the accuracy in the final optical surface reconstruction. For a tungsten ribbon, low order bending modes frequently occur, particularly as the ribbon experiences thermal gradients and load. Thus, the idealized flat rectangular shape of the ribbon, used for data processing and surface reconstruction of deflectometry data measurements, may be incorrect and can lead to surface reconstruction errors. Further, the source output is assumed to be uniform across the ribbon, and stable over the testing period. However, cyclically heated tungsten evaporates and degrades with use over time, leading to a potentially non-uniform emission profile across the surface. This is coupled with the challenge that the ribbon's power draw and emission may fluctuate with time. One final consideration is the limit to how much output power can be achieved with a ribbon source. Because the ribbon acts as a pseudo-blackbody source, increasing the available input power may raise the signal power, but will also shift the output spectrum towards shorter wavelengths, away from the desirable longer wavelength. Above a certain threshold, however, the load will be too great for the ribbon to handle, leading to a failure in the source. These comments are not meant to diminish the impact the tungsten ribbon design had on infrared deflectometry specifically, and metrology generally. Without the introduction of the tungsten ribbon source, high accuracy, rapid and efficient in-situ testing of diffuse optics was challenging, time consuming, and extremely expensive. Instead, these known limitations to the tungsten ribbon lay out a clear framework of considerations that must be addressed to produce an improved infrared deflectometry system at the source level.

We have created a new source design which addresses these prior limitations and opens a new region of infrared deflectometry testing. The source is a Long-wave Infrared Time Modulated Integrating cavity Source (LITMIS), which uses modular high efficiency and high stability resistive membrane blackbody elements. Due to the modular design, the number of elements, referred to as 'caps', inputting radiation into the integrating cavity are readily scalable. The light is output via a machined slit (or any other desired light source pattern geometry), whose geometry is stable and known to high precision machining accuracy. Finally, a key feature of the LITMIS design is the ability to temporarily modulate the source at up to 1 Hz, providing a time-modulated signal, which allows for isolation of the signal from the background noise. The new source was modeled and optimized using illumination design software, and the final optimized design was built and used to measure a diffuse glass and an aluminum blank surface.

Optics EXPRESS

A comparison was made using a traditional deflectometry tungsten ribbon source, whose shape was identical to the exit slit of the box, using the same setup and camera. This allowed for unbiased direct comparison of the two sources. Finally, an aluminum flat under high thermal load, which has historically been unmeasurable using a traditional source due to the low contrast signal for infrared deflectometry and fluctuating background noise, was successfully measured to demonstrate and confirm the high contrast thermal deflectometry performance when utilizing the LITMIS source.

2. Background theory

2.1. Deflectometry

Deflectometry represents a non-null optical metrology method which can, using careful calibration, produce highly accurate surface reconstruction of optics. The metrology method measures the local slope distribution of a unit under test (UUT), and these local slopes are integrated in post-processing to reconstruct the surface map. With proper calibration, deflectometry can provide surface measurements with an accuracy comparable to interferometry [15].

Due to the non-null nature of the test, deflectometry can measure a wide dynamic range of surface slopes. The key limiting factors in a deflectometry test for what is measurable are defined by the source size, the camera field of view (FOV), and whether the tested UUT surface can reflect the light emitted from the source. For an area on the UUT to be testable it must be in the FOV of the camera. Further, by tracing a ray from the camera to any point on the mirror, the ray, following the law of reflection, must then after deflection intercept some point on the source area. This assures that the extent of the source is great enough to fully measure the UUT surface, although techniques exist to assure this can be satisfied for most any surface [16]. Finally, the light emitted from the source must be specularly reflected from the surface of the UUT.

In most deflectometry setups, a high-resolution camera with a well-defined entrance pupil location is used, with the camera entrance pupil location referred to as $c(x,y,z)$. The camera is focused onto the UUT surface, such that the camera pixels are mapped to the UUT surface and represent discrete 'mirror pixels', referred to as $u(x,y,z)$, over which the local slopes will be calculated. Ideally, the source for a deflectometry setup, referred to as $s(x,y,z)$, has well defined spatial emittance, allowing for accurate knowledge of the geometry and has high repeatability and stability. Additionally, it is advantageous to have a source with high signal power, which provides the test system with a high signal-to-noise ratio (SNR). For every camera pixel, the precise location on the source that successfully illuminates the camera pixel is determined during the measurement. Using the ray start location at the source, the end location at the camera, and the intercept location at the mirror pixel, the local slope at the mirror pixel can be determined. This process is extended to all pixels to measure the local slopes at all mirror pixels on the UUT in orthogonal directions, referred to as $S_X(x,y,z)$ and $S_Y(x,y,z)$, representing the x and y slopes respectively. These slope maps are integrated, typically done using a zonal integration method such as Southwell integration [17] or a modal integration such as using a gradient Chebyshev polynomial set [18], resulting in a reconstructed surface map. Figure 1 demonstrates a standard deflectometry setup and the model used for local slope calculation.

Uncertainty in the location of any components in the system will reduce the accuracy of the local slope calculations, and thus the surface reconstruction. Therefore, it is critical to know the exact position and geometry of all components to a high degree of certainty. While this is readily accomplished for the camera, using calibration and measurement methods such as a coordinate measurement machine (CMM) or even a laser tracker, for the source it can be more challenging, as the source is significantly larger than the camera pupil and, in a scanning source design, will have additional mechanical uncertainties. Further, the source emission uniformity and stability are extremely important, as any uncertainty in the source behavior with degrade local slope calculations [14,19]. These issues are readily addressed in visible deflectometry systems, which

Optics EXPRESS

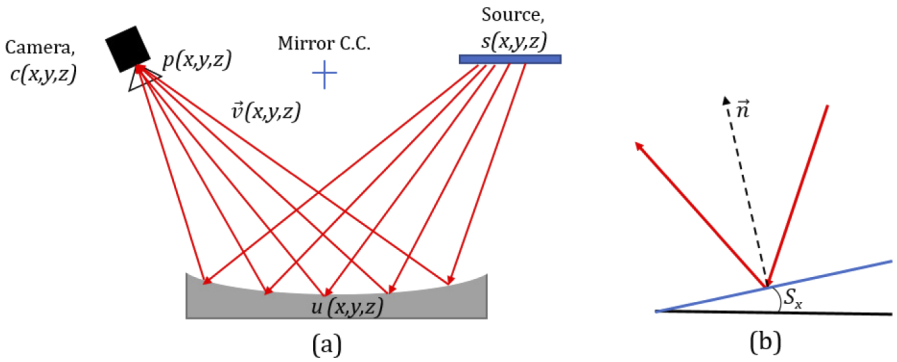

Fig. 1. A traditional deflectometry system relies on a source, $s(x,y,z)$, which emits light with a well-known spatial definition. Some of the light rays, defined as vectors $\vec{v}(x,y,z)$, successfully deflect from the UUT, $u(x,y,z)$, and are captured by a camera, $c(x,y,z)$, whose entrance pupil location, $p(x,y,z)$, is well known. Typically, the source and camera are placed as near to the center of curvature (C.C.) as possible to approach a one-to-one imaging scenario, as shown in (a). By knowing the precise coordinates of the ray origin at the source, the ray intercept at the UUT, and the ray end at the camera, a local slope at the ray intercept can be determined in the x and y directions, referred to as S_X and S_Y respectively. The local surface normal vector $\vec{n}$ with S_x is shown for the local x slope case (b).

benefit from the use of high resolution, high performance digital displays. However, for infrared deflectometry, the problem becomes more challenging.

2.2. Infrared deflectometry

Infrared deflectometry extends deflectometry to measuring diffuse rough optics which are challenging to measure using traditional techniques. There exists a wide range of materials which do not specularly reflect visible light, thus, thermal infrared deflectometry is an important metrology tool. This is particularly true during the grinding phase of mirror fabrication, where a rough grit is used to rapidly grind the UUT down to the final desired surface shape. During this period the root-mean-square (RMS) surface roughness will typically drop from 1000 μm to 1 μm as smaller grit sizes are used. For such rough surfaces, visible light is scattered and thus visible spectrum metrology tools are inapplicable; however, infrared deflectometry has been applied during this phase successfully for several mirror fabrication projects, including the Daniel K. Inouye Solar Telescope (DKIST) primary mirror [7].

The test setup used for most infrared deflectometry systems relies on a rectangular source which is scanned in the x and y orthogonal directions. The longer the emission wavelength of the source, the rougher the surface that can be tested, provided the source power is high enough and a suitable camera for the given wavelength range can be used. Traditionally, a heated tungsten ribbon acts as the source, serving as a pseudo-blackbody element. Coupled with a long-wave infrared (LWIR) camera, which is sensitive in the 7-14 μm range, this allows for testing 1 μm to ~ 25 μm RMS rough surfaces. This test setup has been successfully deployed and used to measure a variety of rough, non-specularly reflecting surfaces and was able to achieve high accuracy surface reconstruction [4,7,14,20]. It should be noted that other dynamic heated screen patterns, including a scanning infrared laser and a resistor array, have successfully been used as sources for infrared systems; however, a heated scanning ribbon still serves as the most common source for testing large diffuse optics [21]. An example case showing the rough 4.2 m diameter off-axis parabola DKIST primary mirror surface during testing, as well as the reflected LWIR light from

Optics EXPRESS

a scanning tungsten ribbon as captured by a LWIR camera for a deflectometry measurement of the UUT are shown below in Fig. 2.

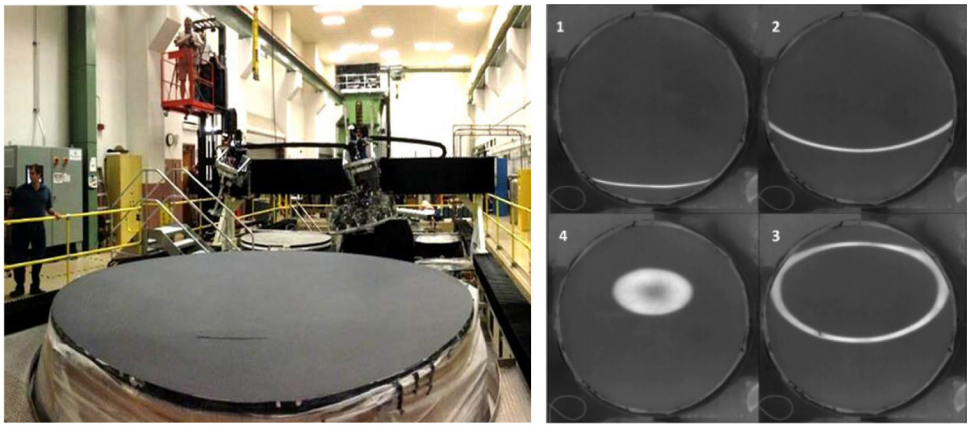

Fig. 2. After generating a mirror blank, the surface goes through a grinding process, which rapidly converges the UUT to the desired shape. For the DKIST primary, a 4.2 m Zerodur blank was ground from ~100 μm down to 1 μm RMS surface roughness. During this process, the rough surface (left) was measured using infrared deflectometry. The infrared deflectometry system uses a scanning heated tungsten ribbon and captures reflected light in the 7-12 μm range during the vertical scan (right), which is specularly reflected by the rough surface. [4]

Just as with visible deflectometry, the uncertainty in all components directly affects the accuracy of the surface reconstruction. In the LWIR region, camera choices are more limited than the visible, with a microbolometer arrays being a common option, which typically have large pixels than CCD or CMOS detectors. However, the diffraction limit in the LWIR region is also approximately an order of magnitude larger than the visible spectrum, thus, the pixel pitch is not a limiting factor. Additionally, accurate knowledge of the source shape and position can become highly challenging if not impossible to measure, as will be explored in the next section.

Finally, the source signal as compared to the background, which broadly is captured by the SNR, is a key characteristic of the source. All objects radiate to some extent in the infrared region; thus, there is a large amount of background thermal radiation both in and out of scene that contributes significantly to the noise levels during an infrared deflectometry test. Further, the background radiation may change during the test. A simple and traditionally used pre-test background image (or average of background images), may not always be enough to remove the background noise during testing. This issue is especially clear when considering that the source itself is moving during the test and may leave a thermal 'tail' in the air, as well as introduce a shifting background emitter in the form of the housing hardware. The noise issue is compounded by the fact that, for a heated metal source, there is a physical limit to how much signal output power can be achieved before failure of the source. Lastly, the output power uniformity and stability are highly important, as any variation during testing will skew results and impart uncertainty into the final reconstructed surface.

3. High contrast deflectometry using LITMIS

3.1. Long-wave infrared time-modulated integrating cavity source

To address the previously covered limitations of a tungsten ribbon source, and to allow for novel testing situation for infrared deflectometry, we have developed LITMIS. The source uses modular

Optics EXPRESS

heating elements as input radiation and has a rectangular output slit where the light is emitted, mimicking the ribbon source dimensions for direct comparison. The cavity and emission area are selected for comparison to a tungsten ribbon source and can be changed and optimized to other geometries for different testing configurations. The design provides high signal output power and temporal stability with uniform emission. Because it is a machined output slit, the source geometry is known to a high machining precision (e.g., ~25 μm) and remains stable over the lifetime of the source.

LITMIS makes use of small resistive caps, which each contain an extremely thin resistive alloy membrane that exhibits high emissivity and can cool extremely quickly [22]. Thus, the source can be temporally modulated, achieving an 80% contrast ratio at 1 Hz. This allows for in-situ updated background noise images during testing, as the signal output can be modulated to capture 'background' and 'signal' images during the scanning. Further, although not implemented in this setup, a detector which provides direct signal output, and does not integrate the signal, can be used to filter the signal in the Fourier domain to further isolate the signal from noise. This approach is not implemented herein due to the available camera in this study.

The integrating cavity can be machined out of any material that maintains shape and diffusely reflects the LWIR being input into the cavity. Consideration of the inner cavity dimensions must be made to assure that the light is properly scattered by the interior surface reflections to achieve a uniform non-directional (i.e., Lambertian) emission from the exit slit. Furthermore, several changes to the LITMIS can be made in order to adjust desired operating performance characteristics:

- Radiant flux: the interior of the cavity may be coated, depending on the cavity material, to adjust the radiant flux by minimizing reflection losses, and the number of input caps can be adjusted to scale radiant flux,
- Output spectrum: the spectral reflectance of the cavity coating and the emission spectrum of the input caps are used to specify the output spectrum at the slit, and
- Output geometry: the emission slit geometry can be altered, although again the interior cavity design must be properly configured to assure proper emission behavior.

With considerations towards matching the geometrical and radiometric properties of a tungsten ribbon source, an integrating cavity source was designed and machined. The cavity is designed with 20 input 'cap' sources, operating at approximately 70% maximum power. The cavity itself is optimized to achieve both angular and spatial uniformity over a rectangular exit, while the interior of the cavity is a box shape made of bare aluminum with a surface roughness of 3.4 μm, measured using a Zygo NewView 8300 Interference Microscope. The design is modeled to match a traditional tungsten ribbon source which has been used in previous infrared deflectometry tests, [23], for comparison purposes. The matching of the slit and ribbon dimensions allows for direct comparison of the two sources. The system is modeled in Synopsys' LightTools, a non-sequential ray tracing simulation software, and the location of the heating elements, as well as interior cavity dimensions and surface roughness, are optimized to achieve spatially uniform, Lambertian radiance over the extent of the exit slit. The output is simulated at the slit with this radiance profile as the goal. The near field irradiance pattern, as well as the final optimized box design, are shown below in Fig. 3.

3.2. Comparative radiometric modeling

For the purposes of a direct comparison, the source power of the integrating cavity design is matched to that of the tungsten ribbon. The tungsten ribbon behaves as a pseudo-blackbody emitting source, and the radiometric equations predicting the ribbon emission are well documented [19]. The LITMIS source can similarly be described as a pseudo-blackbody emitting source.

Optics EXPRESS

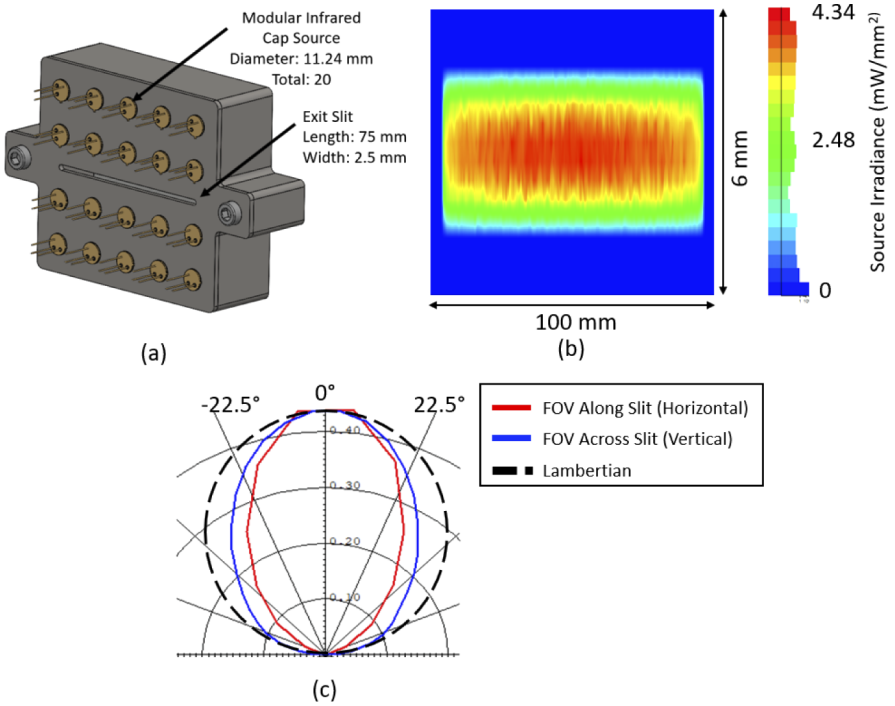

Fig. 3. An aluminum integrating cavity was designed and optimized to make the infrared source, LITMIS. The cavity is designed to have 20 input source ports, where small, high emissivity, modular and time-modulating infrared cap sources are input in the final built box. An emission exit slit, where light exits the box, is designed to match the dimensions of a comparison tungsten ribbon infrared source (a). The optimized design is modeled in LightTools, where the irradiance at the surface of the box is simulated to assure high spatial uniformity across the exit slit (b). The emission intensity as a function of output angle is also analyzed, demonstrating high angular uniformity (c).

Further, each source features the same emission area and are linearly scanned for testing. The raw data acquisition is from the pixel camera detector pixel response, where a centroiding process is used to extract the peak signal response for every camera pixel as a function of source location Thus, as all other components are identical in a system other than the sources, the goal is to match the source radiance.

As has previously been describe [14,24,25], using the law of error propagation, when only noise is considered, the centroid uncertainty, σ, is determined from the recorded intensity response width, w, the number of samples taken, N, and the SNR:

$$\sigma = \frac{w}{\sqrt{N}\ SNR} = \frac{w}{\sqrt{N}\ P_{sig}/NEP} \tag{1}$$

P_{sig} is the signal power and NEP is the noise equivalent power, which is typically the dominant factor in an infrared deflectometry test. The centroid uncertainty, Δs, directly relates to the slope uncertainty as:

$$\Delta s \cong \frac{\sigma}{2Z} \tag{2}$$

where Z is the distance from the source to the UUT. The signal power is determined by considering the reflected radiance, L_{ref}, which is scaled by the transmission of the optical components, given by τ_o, that falls on the detector, whose area given by A_{im}. The image area is related to the source

Optics EXPRESS

width, w_{sc}, and the diameter of the camera aperture, D_{ap}. The solid angle for the pixel from the entrance pupil must also be considered, which is defined as Ω_{pix}, and can be calculated from the area of a single pixel, given as A_{pix}, and the focal length of the camera, given by f. The full signal power equation is given as:

$$P_{sig} = \tau_o L_{ref} A_{im} \Omega_{pix} = \tau_o L_{ref} \ (w_{sc} D_{ap}) \ \frac{A_{pix}}{f^2} \tag{3}$$

The reflected radiance, L_{ref}, is derived from the source radiance, L_{src}, and is scaled by the reflectivity of the UUT, r_U, and the relative reflectance due to rough surface scattering, r_s. The value is calculated according to:

$$L_{ref} = r_U \ r_s \ L_{srce} \tag{4}$$

To this point, the tungsten ribbon and the integrating cavity design share the same radiometric considerations. The primary difference arises in the different source radiance, defined as $L_{src-ribbon}$ and $L_{src-cavity}$ for the ribbon and cavity respectively. The ribbon source radiance is given by

$$L_{srce\_ribbon} = \frac{\varepsilon \ \alpha_{7-14} \ P_{ribbon}}{\pi A_{srce}} \tag{5}$$

where the total power draw, given by P_{ribbon}, is scaled by the emissivity of the source over the given radiation band, ε, which is 0.10 [19,26,27]. For the ribbon configuration used, the power draw was approximately 2.1 W (2.2 A, 0.95 V), with an operating temperature of roughly 440 °C. The portion of the total radiation in the 7-14 µm band, α_{7-14}, is calculated from Stefan-Boltzmann law. Finally, the solid angle is given by $\pi = 3.14$ rad, which is the solid angle when a differential plane source radiates towards a hemisphere and the surface area of the source, A_{src}, is directly calculated from the source geometry. The source radiance for the cavity is similar to that of the ribbon with some minor differences. This is given by:

$$L_{srce\_cavity} = r_c^b \frac{\varepsilon \ \alpha_{7-14} \ P_{tot}}{\Omega_{cavity} A_{srce}} = r_c^b \frac{\varepsilon \ \alpha_{7-14} \ N \ P_{cap}}{\Omega_{cavity} A_{srce}} \tag{6}$$

where the input power is given by the power per cap source, P_{cap}, which for the designed cavity was approximately 0.35 W (23.8 V, 14 mA), with a temperature of 450 °C, and is scaled by the total number of caps inputting energy into the cavity, N, which for the presented design was 20. The product of these two parameters gives the total input power, P_{tot}. The total output radiance from the cavity is scaled by the reflectivity of the cavity interior, r_c, which for bare aluminum at the operating temperature is approximately 0.93 [28] to the power of the average number of bounces taken by a ray from a source cap to exiting the box, b, which for the given design was approximately 46, as calculated in the LightTools model. Finally, the emission solid angle, Ω_{cavity}, is unique to the final cavity design. For the designed cavity for this manuscript, the solid angle is given by 2.43 steradians.

It should be noted that while minor parameters differ between the source radiance definitions for both a heated metal-based source and the LITMIS source, the most fundamental difference is the power scalability of the LITMIS source. Blackbody sources will shift their emission spectrum to higher energy, lower wavelengths as the input power, and thus temperature, increases. This is non-ideal for a long-wave infrared source. Further, there is an input power threshold for all materials, above which the material will fail. As seen in Eq. 6, the same long-wave infrared spectrum can be maintained while adding power to the source by scaling the number of individual emitters, which is a unique feature for the LITMIS source.

The parameter values for the as designed and manufactured LITMIS source, as well the tested tungsten ribbon, are provided in Table 1. The specific details of the source's implementations are provided in later sections.

Optics EXPRESS

Table 1. Source Parameter Comparison between Tungsten Ribbon and LITMIS Sources

Parameter	Notation	Tungsten Ribbon	LITMIS Source	Unit
Total power consumed	P_{tot}	2.10	7	W
Radiation in 7-14 um band	α_{7-14}	0.28	0.28	N/A
Source Emissivity	ε	0.10	0.90	N/A
Cavity Reflectivity	r_c	N/A	0.93	N/A
Internal Ray Bounces	b	N/A	46	N/A
Source Surface Area	A_{src}	1440	1440	mm^2
Source Radiance	L_{srce}	1.36×10^{-5}	1.78×10^{-5}	$W/mm^2/sr$

It must be noted that in the final test, the input power to the cavity and the ribbon were altered slightly to achieve an average identical power signal on a camera pixel from both sources. This is due to the goal of having an unbiased comparison between the two sources; the goal was not to compare the power output from the sources, which can be significantly adjusted via engineering choices.

4. Experimental configuration and measurement setup

An infrared deflectometry system was assembled on an optical table. The camera featured a ~1–2 m variable focal length germanium lens, and the detector was a microbolometer array with 320×240 pixels (7–14 μm response, Thermal-Eye 3500AS). The exposure, gain, and level settings were adjusted prior to testing such that the output was never saturated, and the settings were held constant between all tests. An optical mount was situated approximately one meter from the camera and was fixed in place and allowed for repeatable placed of the UUT. The camera was focused on the UUT surface for deflectometry measurements and was focused on the sources for measurements of the source properties.

For an unbiased performance comparison, the source was the only component in the system which changed during the experimental measurements. To compare properties between source modalities, a scanning platform was utilized with a mounting interface to interchange LWIR sources. A motorized lead screw stage (Velmex BiSlide, Model #MN10-0350-M02-31) moved source assemblies in the vertical direction with an absolute positional accuracy of ± 0.005 mm. For ease of comparison, sources shared identical slit dimensions (75 × 2.5 mm) and radiant exitance planes. Figure 4 demonstrates the camera and source setup for the test system.

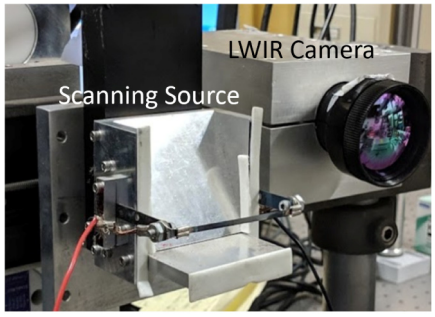

Fig. 4. The infrared testing system used for all tests in this manuscript was composed of a linear scanning source and a long-wave infrared (LWIR) Thermal-Eye 3500AS camera. The source was mounted in a kinematic mount, allowing for repeatable interchange between a tungsten ribbon source, as seen above, and the LITMIS source.

Optics EXPRESS

4.1. Thermal infrared source structure and setup

A LWIR thermal line source was implemented by running direct current (2.2 A, 2.1 W) across a thin tungsten ribbon. Transient thermal noise from the wire, such as the local heating of air, was reduced by taking measurements after the ribbon reached an equilibrium state (~5 minutes), closer to the environmental thermal steady-state condition.

The LITMIS source was implemented by applying a (0.29 A, 7W) load to a circuit consisting of 20 emitters (Axetris Model: EMIRS200 T039 w/ Cap; 2 to 14 μm spectrum, ~ 2π steradian emission). Pointed into the enclosure, the rectangular emitter array was operated by binary power cycling with a digitally controlled relay (Numato 1 Channel USB-Powered Relay Module). Enclosure walls were machined from bare Al 6061-T6 and characterized to 3.4 μm RMS (Root Mean Square) by a Zygo NewView 8300 Interference Microscope. To block excess thermal noise from the slit source aluminum-covered "gull-wing" shields were added. Lastly, to minimize latent thermal radiation from the cavity interior, the LITMIS source was cooled to 0° C prior to each test by placing the source into a cooling chamber for 1 hour prior to testing. Upon removal from the chamber the interior cavity temperature was measured to verify it had reached 0° C, and an image verification was performed to verify that the interior cavity signal counts remained at or below the noise levels of the camera for the duration of each test. Figure 5 demonstrates the integrating cavity after assembly.

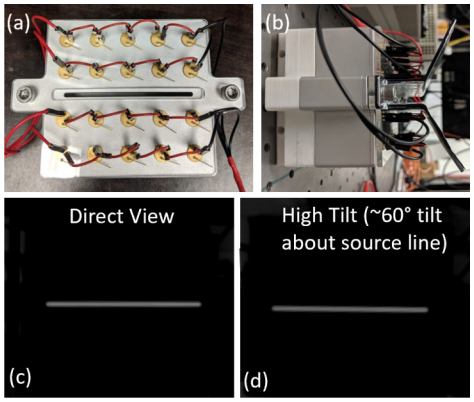

Fig. 5. The assembled LITMIS source was constructed from an aluminum cavity and utilized 20 'cap' input sources (a). Aluminum gull fins were added to the top of the box during testing to shield the back end of the caps and to assure no excess emission or reflected LWIR came from the LITMIS source (b). A direct view of the source, as captured by a LWIR camera, shows high spatial uniformity of the signal and an ideal rectangular emission shape (c), and when the LITMIS source is rotated about the emission slit, the same uniformity and power output is observed (d) indicating non-directional uniform angular emission from the exit slit.

4.2. Unit under test for infrared deflectometry metrology

Two diffuse optics were measured with both the tungsten ribbon and the LITMIS sources. The first optic was a 1500 grit ground glass (BK7) diffusing flat, measuring 2 inches in diameter, referred to as Glass^{1500}. Second, a bare aluminum blank, measuring 3 inches in diameter was tested in two separate configurations. The Al flat was tested at room temperature, referred to as Al_{Room}, and additionally, the optic was tested under thermal load, after being heated to a temperature of 150 °C, referred to as $Al_{150,}$ to simulate/model metrology of an object operating in a high temperature environment such as an aluminum panel slumping process for a Terahertz telescope. The heating was accomplished by placing the aluminum blank on a hot plate operating

Optics EXPRESS

at 150 °C for 30 minutes, at which point the surface temperature was verified as being 150 °C. After which, it was removed from the hot plate and mounted for testing. Surface roughness of the two optics were verified with a Zygo NewView 8300 Interference Microscope. The surface roughness of the Glass_{1500} was measured as 127.89 nm RMS while the Al_{Room} was measured as 102.53 nm RMS. UUTs were positioned 1.35 m from the source plane. Figure 6 demonstrates the UUTs and the surface roughness maps as measured using the white light interferometer.

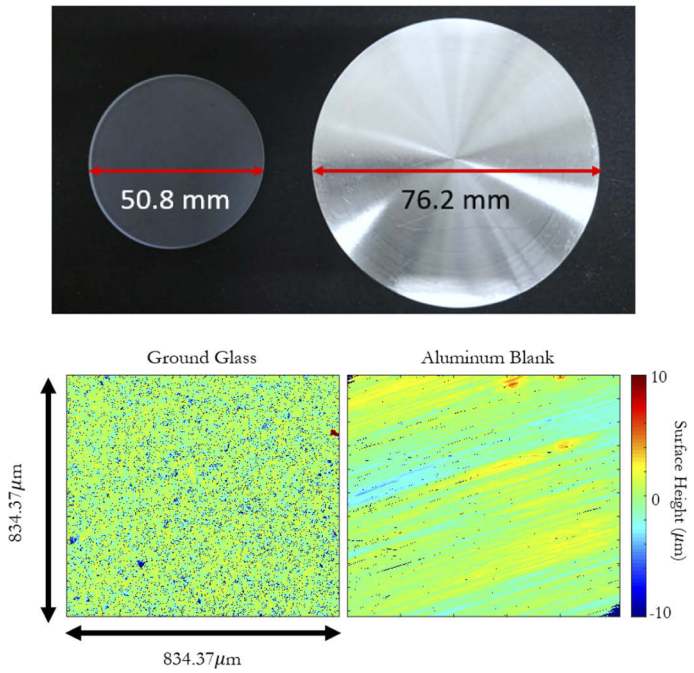

Fig. 6. A 2-inch diameter rough ground glass flat referred to as Glass^{1500} (top left) and a bare aluminum flat referred to as Al_{Room} (top right) were selected for measurement due to their diffuse nature, making thermal infrared deflectometry an ideal metrology method. The surface roughness of both optics was measured using a Zygo NewView 8300 Interference Microscope. The ground glass surface featured a surface roughness of 127.89 nm RMS while the bare aluminum surface roughness was 102.53 nm RMS over a small 834×834 μm square area over each optic (bottom).

4.3. Source geometry and temporal stability measurements

To measure the source emission geometry, tests were performed by recording a focused image of each source using the LWIR camera previously described. A profile across the middle of each source was recorded to determine how similar each true source profile was, as compared to the assumed ideal flat top rectangular emission profile. Consequently, this allowed for verification that the recorded signal power on the camera pixels was similar between the two sources, and that the source area was similar on the detector for both sources.

To observe the temporal stability, a measurement was performed by focusing the camera on each source, which was turned on and recorded for 30 minutes, separately. An image was recorded every 10 seconds. For the test of both the tungsten ribbon source as well as the LITMIS source, signal data was calculated over a series of pixels (50 pixels) that were imaging the source, and the noise statistics were calculated over several random pixels (50 pixels) imaging the background scene. Over every signal pixel the average recorded signal count, the standard deviation of the

Optics EXPRESS

signal, and the peak-to-valley (PV) variation of the signal count, as reported by the output from the detector, was calculated. The mean value for the signal power, referred to as $\text{signal}_{\text{time-mean}}$, the mean standard deviation, referred to as $\text{signal}_{\text{time-std}}$, and the mean PV variation, referred to as $\text{signal}_{\text{time-PV}}$, were calculated. Similarly, the average noise recorded signal over every noise pixel, as well as the standard deviation for every noise pixel was determined. The mean noise signal, referred to as $\text{noise}_{\text{time-mean}}$, as well as the noise standard deviation, referred to as $\text{noise}_{\text{time-td}}$, was also calculated, and is presented in Section 5.1.

4.4. Infrared deflectometry reconstruction and repeatability

To determine the comparative surface reconstruction repeatability, multiple optics were measured using both tungsten ribbon and LITMIS sources. The Glass^{1500} and Al_{Room} and Al_{150} optics were measured using the previously described deflectometry system and the surfaces were reconstructed. For both setups, the source was scanned 150 mm, using 30 interval steps, in a step and stare method. The step-and-stare method was applied, where the source is 'stepped' to the next scan position. Once it has reached the new position and motion is stopped, an image capture is performed, referred to as the 'stare' process. UUT re-mounting and alignment error was avoided by testing surfaces with one source first and then the other, keeping all other system parameters identical between the comparative tests. For all surfaces, 5 measurements were performed in succession at each step and the behavior of several locations across the UUT were analyzed for each source. The centroids were calculated for each source configuration. For the ribbon source, an average of 5 background images were recorded and subtracted from all measurement images. For the LITMIS slit source, an 'on' (cavity emitting light) and 'off' (cavity not emitting light) signal was recorded at every step position, and the 'off' signal at each position was subtracted from the 'on' measurement. After this, a standard centroiding process was used for both source measurements. The total acquisition time for the full 5 successive measurements of each optic was approximately 18 minutes using the tungsten ribbon source and was approximately 20 minutes using the LITMIS slit source.

The repeatability of the source reconstruction was determined by calculating the statistics across the repeated measurements. Across five repeat measurements the recorded peak signal response as well as the standard deviation between measurements of the peak signal response, referred to as $\text{signal}_{\text{mean}}$ and $\text{signal}_{\text{std}}$ respectively, were determined for the camera pixels imaging the UUT. Additionally, the mean peak signal response and standard deviation across the repeat measurements, referred to as $\text{noise}_{\text{mean}}$ and $\text{noise}_{\text{std}}$ respectively, were determined for the camera pixels imaging the background, which represents the noise statistics. The mean signal-to-noise ratio was then determined. Finally, the data for every measurement set was processed and the source coordinate that illuminated every camera pixel imaging the UUT was determined via a standard centroiding process. The mean centroiding uncertainty of the source across the 5 repeated measurements, referred to as δ_{mean} in Table 3.

Taking the processed data, the surface of each optic was reconstructed for every measurement for both sources. Standard Zernike terms were fit to the reconstructed maps, and, after removing terms 1 to 37, the maps were compared. The reconstruction repeatability was analyzed. The results of all tests are detailed in Section 5.2.

5. Experimental data analysis and result

5.1. Source geometry and temporal stability measurements results

The recorded source images the tungsten ribbon and LITMIS sources, captured with the test system LWIR focused through a flat precision mirror onto the source planes, as well as the signal profile across the midline, are shown in Fig. 7.

Optics EXPRESS

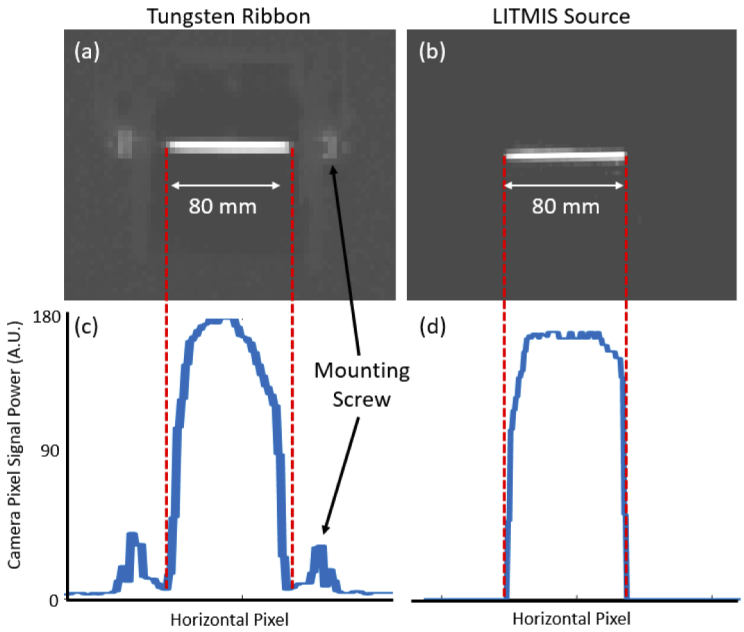

Fig. 7. The source geometry and uniformity are a critical performance defining parameter in a deflectometry system. For the designed infrared deflectometry test system, and image of the tungsten ribbon (a) as well as the LITMIS slit (b) sources was captured using Thermal-Eye 3500AS camera through focused onto the source through a flat mirror. Observing a profile of the source for the tungsten ribbon (c) and the LITMIS slit (d) sources, it is seen that the average signal power is similar, but the source profile geometries are quite different, where both should ideally form a flat top rectangular shape with roll-on and roll-off at the edges due to the convolution of the rectangular source with the circular camera pupil.

The average source signal for both the LITMIS and tungsten ribbon sources, calculated over 50 pixels imaging the source, over a 30-minute period with an image capture every 10 seconds is plotted in Fig. 8.

The results of the source temporal stability measurements are reported and summarized in Table 2. The time averaged camera signal of both sources, referred to as $\text{signal}_{\text{time-mean}}$, was calculated to verify the signal power, as recorded by the camera, was similar for both sources. Further, the standard deviation of the source signal over time, referred to as $\text{signal}_{\text{time-std}}$, is also reported, as is the peak-to-valley signal variation over the 30-minute measurement period, referred to as $\text{signal}_{\text{time-PV}}$. The time averaged background noise signal and the standard deviation of the noise signal over the 30-minute measurement period is reported for both sources, referred to as $\text{noise}_{\text{time-mean}}$ and $\text{noise}_{\text{time-std}}$ respectively.

Table 2. Temporal Stability Comparison between Tungsten Ribbon and LITMIS Slit Sources

Source	$\text{signal}_{\text{time-mean}}$ (A.U.)	$\text{signal}_{\text{time-std}}$ (A.U.)	$\text{signal}_{\text{time-PV}}$ (A.U.)	$\text{noise}_{\text{time-mean}}$ (A.U.)	$\text{noise}_{\text{time-std}}$ (A.U.)
Tungsten Ribbon	95.72	1.97	11.10	72.39	0.45
LITMIS Slit	93.21	0.53	1.82	73.32	0.43

The source image showed similar camera signal readout for both sources, which implies the source radiance for both the LITMIS and tungsten ribbon sources was similar, as designed. However, observing the profile of the sources, the tungsten ribbon source has a peak signal in

Optics EXPRESS

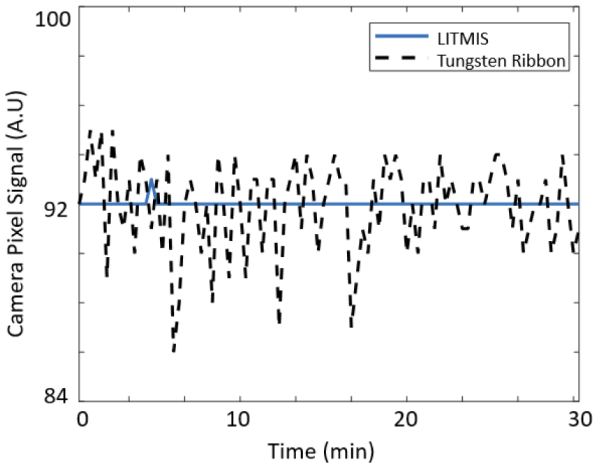

Fig. 8. High temporal stability is essential for a deflectometry source, as any fluctuations in the radiant flux directly impacts the recorded power by the camera pixels, which leads to reconstruction error. Over a 30-minute period, with samples taken every 10 seconds, the camera detector pixel signal of the tungsten ribbon source (dashed black line) and the LITMIS slit (solid blue line) were recorded, to determine temporal stability of both sources.

the middle of the ribbon, which decays towards the edges, while the LITMIS source has a more rectangular emission pattern. The tungsten ribbon deviation from the ideal rectangular pattern is expected as the boundary conditions and material wear will cause the emission pattern to change from ideal. It must be noted that some of the shape deviation from an ideal rectangular shape is due to the limited camera resolution in the test setup, however.

The temporal stability results suggest again that while the average peak signals from both sources are similar, the temporal stability over time is highly different. At a peak mean power of ~95 signal counts on the camera, the tungsten ribbon fluctuated rapidly and randomly ~ 2 camera signal counts, or 2% of the signal power. Further, the peak-to-valley fluctuation at times reached 11 signal counts. The LITMIS slit source had a mean peak power of ~93 signal counts, fluctuating with a standard deviation of ~0.50 signal counts, or 0.5% of the signal power. The peak-to-valley fluctuation was 1.82 counts. In both test cases, the background noise, which is a combination of background radiation and camera noise, fluctuated with a standard deviation of ~0.4 signal counts on the camera. This confirms the superb stability and uniform slit emission geometry of the LITMIS-based solution.

5.2. UUT reconstruction and deflectometry signal repeatability results

The reconstructed surface topology maps of the 2-inch diameter 1500 grit ground glass surface, referred to as Glass^{1500}, as well as the 3-inch diameter aluminum blank tested at room temperature and under a thermal load after being raised to a temperature of 150 °C, referred to as Al_{Room} and Al_{150} respectively are shown in Fig. 9. All surfaces were measured using the same deflectometry system with both the traditional tungsten ribbon source and the LITMIS slit source. The surface roughness was determined by removing Standard Zernike terms 1 to 37 from all surface maps to observe the mid-to-high spatial frequency surface shape terms.

The surface shape error of the Glass^{1500} reconstructed surface was 156.63 nm RMS when tested with the LITMIS source and was 132.33 nm RMS when using the traditional tungsten ribbon source. The surface roughness of the Al_{Room} reconstructed surface was 93.78 nm RMS when measured using the LITMIS source and was 95.63 nm RMS when measured using the tungsten ribbon. The Al_{150} surface was not measurable when using the tungsten ribbon due to the high

Optics EXPRESS

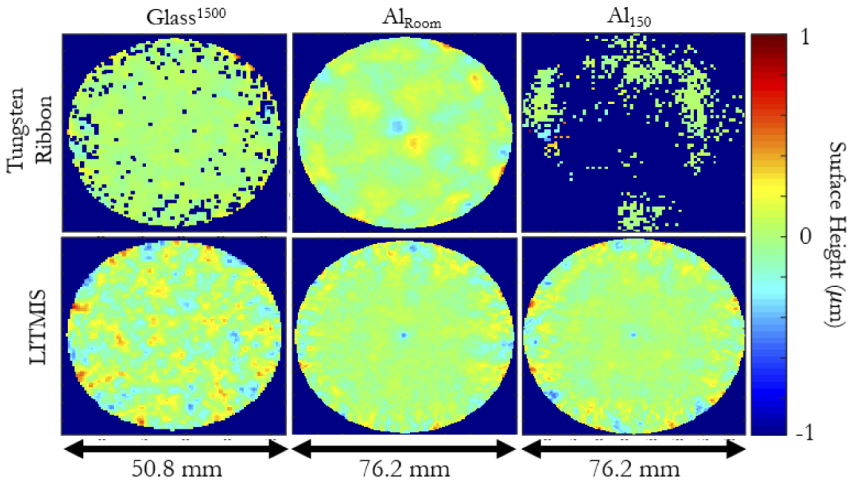

Fig. 9. Using both a traditional tungsten ribbon source (top row) and the LITMIS source (bottom row), infrared deflectometry measurements were taken and the surface reconstructed for the $Glass^{1500}$ optic (left column), the Al_{Room} optic (middle column), and the Al_{150} optic (right column). For all maps, Standard Zernike terms 1:37 were removed to observe the surface mid-to-high spatial frequency topology.

thermal background noise from the heated UUT itself. However, due to the high contrasts signal via the time modulations of LITMIS slit source, the surface shape was successfully measured with the LITMIS source with a value of 106.65 nm RMS.

The signal from one pixel measuring the Al_{Room} surface during the five repeat measurements using the LITMIS source, as well as the average signal response is shown in Fig. 10. The mean peak signal response and the standard deviation of the peak signal response, as well as the mean peak background noise and standard deviation of the noise across the five measurements is also shown.

A frame of the raw signal recorded by the camera during the testing of the Al_{Room} optic, as captured when using both the LITMIS and tungsten ribbon sources, as well as the background subtracted processed data, is shown in Fig. 11. A full video of the entire vertical scan of the optic, for both sources, is provided in Visualization 1.

The signal, noise, and centroiding repeatability results across the five repeat deflectometry measurements of all optics, using both the LITMIS slit and tungsten ribbon sources, are summarized in Table 3. Please note that due to the lack of signal and the large noise in the measurement of the Al_{150} surface with a tungsten ribbon, it was impossible to record a consistent signal over anything more than a small portion of the UUT surface. Thus, these results were omitted as the signal, noise, SNR, and centroiding error could not be calculated.

Both the LITMIS slit source and tungsten ribbon source were successfully used to test the $Glass^{1500}$ and Al_{Room} optics. In both test cases, the mean signal power recorded after reflection from the optic was similar. The standard deviation across the five repeat measurements performed for every optic using each source however was slightly larger for the tungsten ribbon as compared to the LITMIS source. The LITMIS slit source was better able to reduce noise, with an average background noise of 0.70 camera signal counts in the glass test case, as compared to 1.28 counts for the tungsten ribbon, and approximately 0.85 counts for the tests of the aluminum blank, as compared to 4.74 counts for the tungsten ribbon. This directly impacts the SNR of both test methods, with the LITMIS slit source achieving a 2 - 5 times larger SNR. The centroiding repeatability over the five tests, determined by calculating the standard deviation of

Optics EXPRESS

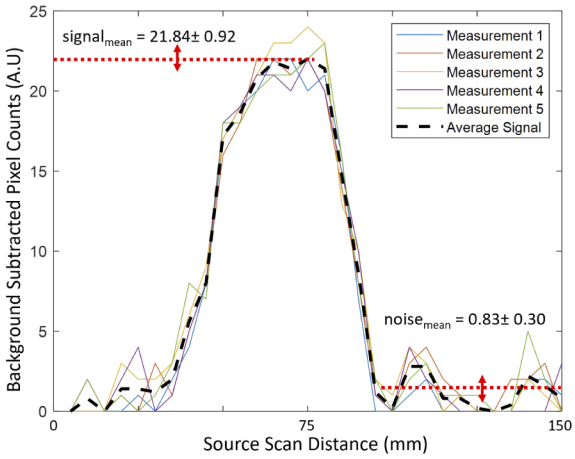

Fig. 10. Five repeat measurements were obtained for every source configuration testing every optic. The five repeat camera signals for one pixel imaging the aluminum blank at room temperature during testing using the LITMIS source were plotted, along with the average signal across the five measurements. For this test the mean peak signal recorded was 21.84, with a standard deviation of 0.92, while the mean peak background noise signal was 0.83, with a standard deviation of 0.30.

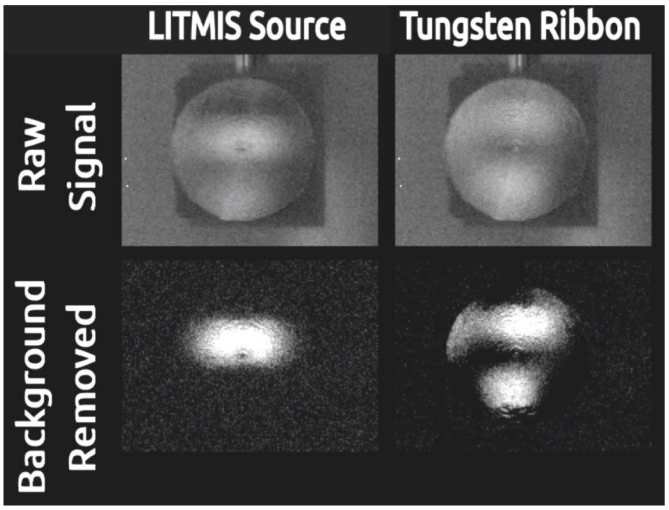

Fig. 11. The deflectometry measurement of the Aluminum blank had the Thermal-Eye 3500AS camera focused onto the UUT surface. The camera recorded an image of the UUT every at every source stage scanning position. This process was done with both the LITMIS slit source (left column) and tungsten ribbon source (right column), which resulted in a raw data signal (top row). The background signal was then removed from the data, using signal isolation for the LITMIS slit source and simple background subtraction for the tungsten ribbon, resulting in a background removed processed signal (bottom row). For the full video of the vertical scan, see Video 1.

Optics EXPRESS

Table 3. Deflectometry Signal and Reconstruction Statistics

Source	Optic	$signal_{mean} \pm signal_{std}$ (A.U.)	$noise_{mean} \pm noise_{std}$ (A.U.)	SNR	Centroiding Error, δ_{mean} (scan step)
Tungsten Ribbon	$Glass^{1500}$	4.68 ± 1.92	1.28 ± 0.44	3.66	1.26
LITMIS Slit	$Glass^{1500}$	5.32 ± 0.94	0.70 ± 0.26	7.60	0.30
Tungsten Ribbon	Al_{Room}	22.68 ± 1.17	4.74 ± 0.27	4.78	1.00
LITMIS Slit	Al_{Room}	21.84 ± 0.92	0.85 ± 0.30	25.69	0.26
Tungsten Ribbon	Al_{150}	Not Measurable			
LITMIS Slit	Al_{150}	18.44 ± 0.81	0.89 ± 0.27	20.71	0.27

the centroids, was consistently approximately a third of a scan step for the LITMIS source and was approximately a full scan step for the tungsten ribbon source.

We acknowledge that the surface reconstruction results are in no way meant to reflect the reconstruction accuracy of either source, as the reconstruction accuracy is related to several system level effects and not the scope of the presented work. The performance and accuracy of an infrared deflectometry system using a tungsten ribbon has been already confirmed and published [14,19]. The significance of the LITMIS solution is demonstrated by observing and comparing the repeatability and noise statistics of the traditional tungsten ribbon source and the LITMIS source.

6. Conclusion

While infrared deflectometry has been used to provide metrology of rough surfaces, there are clear limitations in surface testing and reconstruction capabilities due to inherent characteristics of a tungsten ribbon source. For precision fabrication and metrology, any uncertainty in the spatial and temporal behavior of a source directly negatively impacts the reconstruction accuracy and uncertainty. Additionally, due to testing being performed in the infrared region, there are almost always significant background thermal radiation contributions, which may fluctuate over time and further degrade results. We have instead created an integrating cavity source, which emits long-wave infrared light uniformly from a precision machined exit slit, which we call LITMIS. The temporal and spatial emission behavior is excellent for the source. Further, the source is temporally modulated at up to 1 Hz, which allows not only for better signal isolation from the background noise but can accommodate testing in an environment where background thermal fluctuations are occurring.

A demonstration infrared deflectometry system using the new LITMIS slit source successfully tested a diffuse ground glass optic as well as an aluminum blank. The source exhibited excellent repeatability and significantly improved the SNR of the test, as compared to testing using a traditional tungsten ribbon. Further, the LITMIS slit source allowed for testing a previously unmeasurable aluminum blank while under thermal load, with the blank having been heated to approximately 150 °C. This could enable in-situ testing of optics placed under thermal load to observe surface behavior in extreme environment situations. We do not claim using the LITMIS method is a superior test method to other metrology solutions. Instead, our goal is to expand the library of usable infrared sources for deflectometry, thereby further expanding the metrology options.

Acknowledgment

This research was made possible in part by the II-VI Foundation Block-Gift Program, the Technology Research Initiative Fund Optics/Imaging Program, and the Friends of Tucson Optics

Optics EXPRESS

Endowed Scholarships in Optical Sciences. Additionally, the non-sequential light modeling and analysis was made possible by the educational license for LightTools provided by Synopsys.

References

1. D. W. Kim, H. M. Martin, and J. H. Burge, "Calibration and optimization of computer-controlled optical surfacing for large optics," in *Optical Manufacturing and Testing IX* (International Society for Optics and Photonics, 2011), 8126, p. 812615.
2. M. Beier, S. Scheiding, A. Gebhardt, R. Loose, S. Risse, R. Eberhardt, and A. Tünnermann, "Fabrication of high precision metallic freeform mirrors with magnetorheological finishing (MRF)," in *Optifab 2013* (International Society for Optics and Photonics, 2013), 8884, p. 88840S.
3. T. Blalock, K. Medicus, and J. D. Nelson, "Fabrication of freeform optics," in *Optical Manufacturing and Testing XI* (International Society for Optics and Photonics, 2015), 9575, p. 95750H.
4. D. W. Kim, C. Oh, A. Lowman, G. A. Smith, M. Aftab, and J. H. Burge, *Proc. SPIE 9912, Advances in Optical and Mechanical Technologies for Telescopes and Instrumentation II*, 99120F (22 July 2016);
5. D. W. Kim, J. H. Burge, J. M. Davis, H. M. Martin, M. T. Tuell, L. R. Graves, and S. C. West, "New and improved technology for manufacture of GMT primary mirror segments," in *Advances in Optical and Mechanical Technologies for Telescopes and Instrumentation II* (International Society for Optics and Photonics, 2016), 9912, p. 99120P.
6. P. Zhou, H. Martin, C. Zhao, and J. H. Burge, "Mapping distortion correction for GMT interferometric test," in *Imaging and Applied Optics Technical Papers (2012)*, Paper OW3D.2 (Optical Society of America, 2012), p. OW3D.2.
7. C. J. Oh, A. E. Lowman, G. A. Smith, P. Su, R. Huang, T. Su, D. Kim, C. Zhao, P. Zhou, and J. H. Burge, "Fabrication and testing of 4.2 m off-axis aspheric primary mirror of Daniel K. Inouye Solar Telescope," in *Advances in Optical and Mechanical Technologies for Telescopes and Instrumentation II* (International Society for Optics and Photonics, 2016), 9912, p. 99120O.
8. M. B. Dubin, P. Su, and J. H. Burge, "Fizeau interferometer with spherical reference and CGH correction for measuring large convex aspheres," Proc. SPIE **7426**, 74260S (2009).
9. R. Geyl, D. Bardon, R. Bourgois, N. Ferachoglou, E. Harel, and C. Couteret, "First steps in ELT optics polishing," in *Fifth European Seminar on Precision Optics Manufacturing* (International Society for Optics and Photonics, 2018), 10829, p. 1082904.
10. M. Dimmler, P. Barriga, M. Cayrel, F. Derie, A. Foerster, F. Gonte, J. C. Gonzalez, L. Jochum, N. Kornweibel, S. Leveque, C. Lucuix, and L. Pettazzi, "Getting ready for serial production of the segmented 39-meter ELT primary: status, challenges and strategies," in *Ground-Based and Airborne Telescopes VII* (International Society for Optics and Photonics, 2018), 10700, p. 1070043.
11. U. Mueller, "Production metrology design and calibration for TMT primary mirror fabrication used at multiple manufacturing sites," in *Ground-Based and Airborne Telescopes VI* (International Society for Optics and Photonics, 2016), 9906, p. 99060Z.
12. M. Sieger, F. Balluff, X. Wang, S.-S. Kim, L. Leidner, G. Gauglitz, and B. Mizaikoff, "On-chip integrated mid-infrared GaAs/AlGaAs mach–zehnder interferometer," Anal. Chem. **85**(6), 3050–3052 (2013).
13. H. Yoo, G. A. Smith, C. J. Oh, A. E. Lowman, and M. Dubin, "Improvements in the scanning long-wave optical test system," in *Optical Manufacturing and Testing XII* (International Society for Optics and Photonics, 2018), 10742, p. 1074216.
14. T. Su, S. Wang, R. E. Parks, P. Su, and J. H. Burge, "Measuring rough optical surfaces using scanning long-wave optical test system. 1. Principle and implementation," Appl. Opt. **52**(29), 7117–7126 (2013).
15. H. M. Martin, R. G. Allen, J. H. Burge, J. M. Davis, W. B. Davison, M. Johns, D. W. Kim, J. S. Kingsley, K. Law, R. D. Lutz, P. A. Strittmatter, P. Su, M. T. Tuell, S. C. West, and P. Zhou, "Production of primary mirror segments for the Giant Magellan Telescope," in *Advances in Optical and Mechanical Technologies for Telescopes and Instrumentation* (International Society for Optics and Photonics, 2014), 9151, p. 91510J.
16. L. R. Graves, H. Quach, H. Choi, and D. W. Kim, "Infinite deflectometry enabling 2pi-steradian measurement range," Opt. Express **27**(5), 7602–7615 (2019).
17. W. H. Southwell, "Wave-front estimation from wave-front slope measurements," J. Opt. Soc. Am. **70**(8), 998–1006 (1980).
18. M. Aftab, J. H. Burge, G. A. Smith, L. Graves, C. Oh, and D. W. Kim, "Chebyshev gradient polynomials for high resolution surface and wavefront reconstruction," in *Optical Manufacturing and Testing XII* (International Society for Optics and Photonics, 2018), 10742, p. 1074211.
19. T. Su, *Asphercial metrology for non-specular surfaces with the Scanning Long-wave Optical Test System* (2014).
20. D. W. Kim, T. Su, P. Su, C. Oh, L. Graves, and J. Burge, "Accurate and rapid IR metrology for the manufacture of freeform optics" http://www.spie.org/newsroom/6015-accurate-and-rapid-ir-metrology-for-the-manufacture-of-freeform-optics?SSO=1.
21. S. Höfer, J. Burke, and M. Heizmann, "Infrared deflectometry for the inspection of diffusely specular surfaces," Adv. Opt. Techn. **5**(6), 377–387 (2016).

Optics EXPRESS

22. T. Hessler, O. Dubochet, M. Forster, M. Merschdorf, and P. Surbled, "Micro-machined, electrically modulated thermal infrared source with black body characteristic," in *8th International Conference and Exhibition on Infrared Sensors & Systems* (2004), 1.
23. T. Su, W. H. Park, R. E. Parks, P. Su, and J. H. Burge, "Scanning Long-wave Optical Test System: a new ground optical surface slope test system," in *Optical Manufacturing and Testing IX* (International Society for Optics and Photonics, 2011), 8126, p. 81260E.
24. P. R. Bevington and D. K. Robinson, *Data Reduction and Error Analysis for the Physical Sciences* (McGraw-Hill, 2003).
25. J. S. Morgan, D. C. Slater, J. G. Timothy, and E. B. Jenkins, "Centroid position measurements and subpixel sensitivity variations with the MAMA detector," Appl. Opt. **28**(6), 1178–1192 (1989).
26. J. C. De Vos, "A new determination of the emissivity of tungsten ribbon," Physica **20**(7-12), 690–714 (1954).
27. V. D. Dmitriev and G. K. Kholopov, "Radiant emissivity of tungsten in the infrared region of the spectrum," J. Appl. Spectrosc. **2**(6), 315–320 (1965).
28. K. Ujihara, "Reflectivity of metals at high temperatures," J. Appl. Phys. **43**(5), 2376–2383 (1972).

130.135.185.90 {ts '2019-09-23 13:18:10'}